Timescales of influenza A/H3N2 antibody dynamics

Adam J. Kucharski[1*], Derek A. T. Cummings[2], Steven Riley[3]

[1]Centre for the Mathematical Modelling of Infectious Diseases, London School of Hygiene & Tropical Medicine, UK. [2]Emerging Pathogens Institute, University of Florida, Gainesville, FL 32610, USA. [3]MRC Centre for Outbreak Analysis and Modelling, Department of Infectious Disease Epidemiology, School of Public Health, Imperial College London, UK.

*To whom correspondence should be addressed. Email: adam.kucharski@lshtm.ac.uk.

Abstract

Human immunity shapes the evolution and impact of novel influenza strains. However, it is challenging to quantify the mechanisms that shape observed immune responses or reliably estimate infection from serology because individuals are infected with multiple strains during their lifetime. Using a Bayesian model of antibody dynamics at different timescales, we explain complex cross-reactive antibody landscapes by inferring participants' histories of infection with serological data from studies in southern China and Vietnam. We show antibody profiles are generated by a short-lived, broadly cross-reactive response that decays to leave a long-term response acting against a narrower range of strains. We also suggest an alternative to seroconversion for the estimation of infection attack rates. Our work provides a general method for elucidating mechanisms of influenza immunity from serological data, and suggests a two-armed immune response to influenza infection consistent with competitive dynamics between acute and convalescent B cell populations.

Main text

Immunity against influenza A can influence the severity of disease (*1, 2*), the effectiveness of vaccination strategies (*3*), and the emergence of novel strains (*4, 5*). Understanding the accumulation of immunity and infection has proven challenging because observed human antibody responses – as measured by haemagglutination inhibition assays or microneutralisation titres – reflect a combination of past infections to specific strains and the potentially cross-reactive responses generated by these infections (*6*). Although there are established techniques for the analysis of single strain immunising pathogens such as measles (*7*), potential cross-reactivity between different influenza A strains means serological analysis must account for the dynamics of antibody responses across multiple infections (*8*). The concept of an antibody landscape has been put forth to represent the immune response developed as a result of a sequence of processes such as infection, antibody boosting, antibody waning and cross reactivity (*9*).

Previous work has used cross-sectional data to explore the life course of immunity by explicitly modelling both the processes of infection and immunity (*10*). However, such analysis could not examine antibody mechanisms operating at multiple time-scales. In particular, there have been suggestions that influenza infection leads to 'back-boosting', generating a broadly cross-reactive response against historical strains (*9, 11, 12*). It has also been suggested that influenza responses are influenced by antigenic seniority, with strains seen earlier in life shaping subsequent antibody responses (*13*). This is a refinement on the earlier concept of 'original antigenic sin', whereby the largest antibody response is maintained against the first infection of a lifetime (*14*).

To quantify antibody kinetics over time and estimate historical infections with influenza A/H3N2, we used a dynamic model of immune responses that generated expected titres against specific strains (*10*) by combining infection history – which was specific for each individual – with an antibody response process that was universal across individuals. We assumed that the response included both a short-term and long-term component. The short-term component consisted of a boost in log-titre following infection, which decayed over time, as well as a rise in log-titre as a result of cross-reaction with antigenically variable strains. The long-term response featured a boost in log-titre, which did not decay, and a separate cross-reaction process that led to increased titres against other strains. Titres were also influenced by antigenic seniority, with later infections generating lower new titres than those generated against strains encountered earlier in life (*15*).

We fitted this model to two publicly available serological datasets in which participants were tested against a panel of A/H3N2 strains. The first contained cross-sectional data for individuals living in Guangdong province in southern China, collected in 2009 (*13, 16*); the second included longitudinal data from Ha Nam in Vietnam (*17*), with sera collected between 2007–2012 (*9*). Historical strains were assumed to follow a smooth path through a two-dimensional antigenic space over time (*18*) (Fig. S1). Although the contributions of short- and long-term processes to antibody responses cannot be robustly estimated from cross-sectional data (*10*), simulation studies showed that both time scales were identifiable using a simulated dataset similar to that of the Vietnam samples (Figs. S2–3); we included the short-term dynamic antibody processes in the model when fitting longitudinal data, but not when fitting to cross-sectional data.

We jointly estimated influenza infection history for each study participant, as well as subsequent antibody response processes and assay measurement variability. The fitted model could reproduce both cross-sectional and longitudinal observed titres for each participant (Fig. 1), and it was possible to identify specific years with a high probability of infection and the corresponding antibody profile this infection history had generated (Table S1, Figs. S4–5). Using the longitudinal Vietnam data, we could identify specific years in which individual's had a high probability of infection, particularly during the period of testing (Fig. 1A–I). There was more variability in estimates from the cross-sectional China data, although time periods with a high probability of infection could still be identified (Fig. 1J–L).

The model fits to longitudinal data describe an antibody response to influenza that is initially dominated by a broadly cross-reactive response, which rapidly decays, leaving a long-term response that cross-reacts only with antigenically similar viruses (Table S2, Figs. S6–7). We estimated that primary infection generated a short-lived boost of an average of 2.69 (95% CrI: 2.50–2.89) units of log-titre against the infecting virus (a four-fold rise would be equivalent to a 2 unit rise in log-titre), and a long-term boost of 1.80 log-titre units (95% CrI: 1.74–1.88). The short-term response decayed quickly: we estimated that the response had reached its final equilibrium level after one year. As the samples were collected at one year intervals, it was not possible to estimate beyond this level of precision. The timescale of the response is consistent with previous qualitative estimates based on laboratory confirmed infections, which suggested there was a negligible change in titre more than one year post-infection (*9, 11, 19*).

For the long-term response inferred from longitudinal data, we estimated that cross-reaction between infecting virus and strains tested in the serological assay led to a drop of 0.241 units of log-titre (95% CrI: 0.228–0.261) with every unit of antigenic distance from the infecting strain. We obtained a similar finding using the cross-sectional China data, with log-titres decreasing by 0.182 (0.116-0.237) with each antigenic unit. The broader credible interval for China is largely the result of the coverage of strains tested: 9 strains were tested in the China data, compared with up to 57 in the Vietnam data. For the broader short-term response, the model fitted to longitudinal data suggested cross-reactive titres only decreased by 0.088 (95% CrI: 0.074–0.101) with each antigenic unit. This result suggests that short-term titres are influenced by antigenic distance, albeit weakly, and hence provides quantitative support for previous suggestions that the observed broad short-lived boost is part of a memory B cell response (*9*). This short-lived broad response, which we estimated makes the largest contribution to titres following infection, may also influence selection pressure imposed on the virus as a result of population immunity; it has been suggested that such short-term nonspecific immunity could explain the constrained genetic diversity of circulating influenza viruses (*4*).

Building on previous modelling analyses (*10, 13, 20, 21*), these results suggest that non-primary influenza exposures generate a short-lived broad humoural response and a persistent narrow response, with each degrading to different degrees over the course of a human lifetime. These mechanisms could be observed directly using modern methods of sorting and sequencing individual B cells (*22*). During non-primary infections, existing well-differentiated memory B cells generated during prior infections are rapidly stimulated. These B cells may reach high peripheral frequencies rapidly but, on average, have lower avidity against the current strain than they would have had against that host's previous infections (*23*). They would be well-differentiated from germline B cells, would not differentiate further if observed later in infection, and would form numerous phylogenetic clades. The long-lived persistent response comes from the stimulation of germline B cells which may take longer to achieve functional peripheral frequencies but have higher avidity (*24*). When observed during early infection, these cells would be much more similar to germline B cells, and would form fewer phylogenetic clades per sorted cell than the rapid response. Later during infection, cells making up the persistent response would be at higher frequencies and be more differentiated, but still form only few clades. Antigenic seniority (*13*) may arise because novel lineages during later life infections have to com-

pete with existing lineages for antigenic stimulation (*25, 26*). After infection, the memory frequency of the B cells making up the broad response likely returns to their pre-infection levels and the new B cells establish new subordinate memory populations. The aggregate effect of these mechanisms over a lifetime is consistent conceptually with our HI-based results presented here (Fig. S8).

To illustrate the inferred short and long term antibody dynamics against A/H3N2, we used our mechanistic model to simulate antibody responses following two sequential infections, the first in 1968 and in 1988 (Fig. 2). Following primary infection, individuals would be expected to have raised titres to strains in nearby regions of antigenic space, but these titres would quickly decay to leave a more localised long-term response. Upon secondary infection, a similar boost in titres would be observed, which would not be present in tests conducted in subsequent years. This highlights the importance of accounting for multiple-time scales when analysing immune assay data: in simulations, serology taken in 1988 indicated a rise in titre to the first infecting strain compared to serology between 1969–1987, and showed detectable titres against all strains in the region of antigenic space between the two infecting strains (Fig. 2F). However, serology taken one year later only displayed localised responses against the infecting strains (Fig. 2H). Depending on time of sampling, our results suggests it would be possible to observe either longitudinal increases or decreases in log-titres against previously seen strains or stable log-titres (*6*).

The multiple timescales of the immune response would also have implications for use of serology to investigate the evolutionary dynamics of influenza, and hence identify potential vaccine strain candidates (*20, 27*). If a large proportion of a population had recently experienced infection, it is likely that the short term response would protect these individuals against strains occupying a nearby region of antigenic space. However, these strains may become more transmissible as the short-term response wanes. Therefore our analysis illustrates the temporal response that would be expected if highly valent and immunogenic vaccines were adapted to target a broader range of antigenic space (*9*). At best, such vaccination against influenza A/H3N2 may stimulate a similar response to natural infection. However, there is evidence that vaccine-mediated immunity wanes quickly (*28*), that vaccine effectiveness declines after multiple infections (*29*), and that broad response fades after repeated vaccination (*30*). It has also been suggested that prior natural infection boosts vaccine responses against antigenically drifted strains, but prior vaccination does not (*31*). With appropriate data on serology and vaccination history

in other populations, the differences in dynamics between the two processes could be elucidated using the model structure we have presented here.

As well as examining antibody dynamics, we also reconstructed historical annual attack rates (Fig. 3A). In simulation studies, estimates of attack rates based on the traditional gold-standard of a four-fold rise in titre typically underestimated the actual simulated values (Fig. 3B, inset), and an overestimate was obtained if a two-fold rise in titre was considered instead (*32*). In contrast, estimates from our joint inference framework recovered the true simulated infection dynamics during the period of sampling. Similarly, when our joint inference framework was applied to real data from Vietnam, estimates were consistent with observed epidemiological dynamics in Vietnam between 2008–2012, as measured by the number of influenza A/H3N2 isolates during the testing period (Fig. 3B, main panel). The correlation between model estimates and observed values was ρ=0.996 ($p<0.001$), with a weaker association when a two-fold rise (ρ=0.862, p=0.14) or four-fold rise (ρ=0.799, p=0.20) was used to estimate attack rates. Most of the uncertainty in attack rate estimates resulted from individuals with multiple estimated infections; there was little variation in estimated number of infections when individuals had fewer than around eight median infections (Fig. 3C). Our results suggest that joint estimation of infection history and antibody dynamics could provide more accurate information about infection rates, particularly in the years preceding sample collection (Fig. S2). Such approaches could be employed during evaluation of the effectiveness of vaccination strategies, which depend on an ability to reliably infer population attack rates.

Our analysis shows that detailed mechanistic insights can be gained from longitudinal data by jointly considering individual infection histories and antibody dynamics acting at multiple timescales. This inference approach could therefore be used in future to guide design of studies to infer key aspects of antibody dynamics or to estimate historical attack rates. Further, the results suggest accounting for both short- and long-term humoural responses to influenza will be crucial in designing studies to examine the role of vaccination on population immunity profiles, and subsequent impact on evolutionary dynamics. Our approach is also likely to be applicable to other cross-reactive pathogens, such as dengue fever and Zika viruses (*33*).

References

1. K. M. Gostic, M. Ambrose, M. Worobey, J. O. Lloyd-Smith, *Science* **354**, 722 (2016).
2. E. Miller, *et al.*, *The Lancet* **375** (2010).
3. M. Baguelin, *et al.*, *PLOS Medicine* **10** (2013).
4. N. M. Ferguson, A. P. Galvani, R. M. Bush, *Nature* **422**, 428 (2003).
5. J. C. Jones, *et al.*, *J Virol* **88**, 1175 (2014).
6. M. S. Miller, *et al.*, *Sci Transl Med* **5** (2013).
7. B. Grenfell, R. Anderson, *Epidemiology and Infection* **95**, 419 (1985).
8. D. N. Vinh, M. F. Boni, *Epidemics* **12**, 30 (2015).
9. J. Fonville, *et al.*, *Science* **346**, 996 (2014).
10. A. J. Kucharski, *et al.*, *PLoS Biology* **13**, e1002082 (2015).
11. F. Horsfall, E. Rickard, *The Journal of Experimental Medicine* **74**, 433 (1941).
12. J. Lessler, *Science* **346**, 919 (2014).
13. J. Lessler, *et al.*, *PLoS Pathog* **8**, e1002802 (2012).
14. T. Francis Jr., *Proceedings of the American Philosophical Society* **104**, 572 (1960).
15. See supplementary information.
16. J. Lessler, *et al.*, *Nat Commun* **2**, 423 (2011).
17. P. Horby, *et al.*, *Am J Epidemiol* **175**, 1062 (2012).
18. D. J. Smith, A. S. Lapedes, J. C. de Jong, *et al.*, *Science* **305**, 371 (2004).
19. J. P. Hsu, *et al.*, *BMC infectious diseases* **14**, 414 (2014).
20. S. Cobey, S. E. Hensley, *Current Opinion in Virology* **22**, 105 (2017).
21. V. I. Zarnitsyna, J. Lavine, A. Ellebedy, R. Ahmed, R. Antia, *PLoS Pathog* **12**, e1005692 (2016).

22. H.-X. Liao, *et al.*, *Nature* **496**, 469 (2013).

23. J. Wrammert, *et al.*, *J Exp Med* **208**, 181 (2011).

24. J. G. Petrie, *et al.*, *J. Infect. Dis.* **214**, 1947 (2016).

25. S. G. Tangye, D. T. Avery, E. K. Deenick, P. D. Hodgkin, *The Journal of Immunology* **170**, 686 (2003).

26. J. Kim, I. Skountzou, R. Compans, J. Jacob, *The Journal of Immunology* **183**, 3294 (2009).

27. World Health Organisation, *who.int* (2010).

28. E. Kissling, *et al.*, *Eurosurveillance* **21** (2016).

29. H. Q. McLean, *et al.*, *Clinical Infectious Diseases* **59**, 1375 (2014).

30. S. F. Andrews, *et al.*, *Science Translational Medicine* **7**, 316 (2015).

31. J. H. Kim, *et al.*, *Vaccine* **34**, 495 (2016).

32. S. Cauchemez, *et al.*, *PLoS Pathog* **8**, e1003061 (2012).

33. A. J. Kucharski, S. Riley, *Lancet Infect Dis* **17**, 13 (2017).

34. G. Gibson, E. Renshaw, *Mathematical Medicine and Biology* **15**, 19 (1998).

35. G. O. Roberts, J. S. Rosenthal, *Journal of Computational and Graphical Statistics* **18**, 349 (2009).

36. C. Jackson, E. Vynnycky, P. Mangtani, *American Journal of Epidemiology* pp. 465–78 (2009).

37. WHO, *FluNet* (Global Influenza Surveillance Network, 2012).

Acknowledgements A.J.K. was supported by the Medical Research Council (fellowship MR/K021524/1). S.R was supported by the Medical Research Council (UK, Project MR/J008761/1), Wellcome Trust (093488/Z/10/Z, 200861/Z/16/Z, 200187/Z/15/Z), National Institute for General Medical Sciences (MIDAS U01 GM110721-01), National Institute for Health Research (UK, for Health Protection Research Unit funding). We would also like to thank Justin Lessler and Hua-Xin Liao for helpful discussions.

Supplementary materials

Materials and Methods

Figs. S1 to S10

Tables S1 to S2

References *(34–37)*

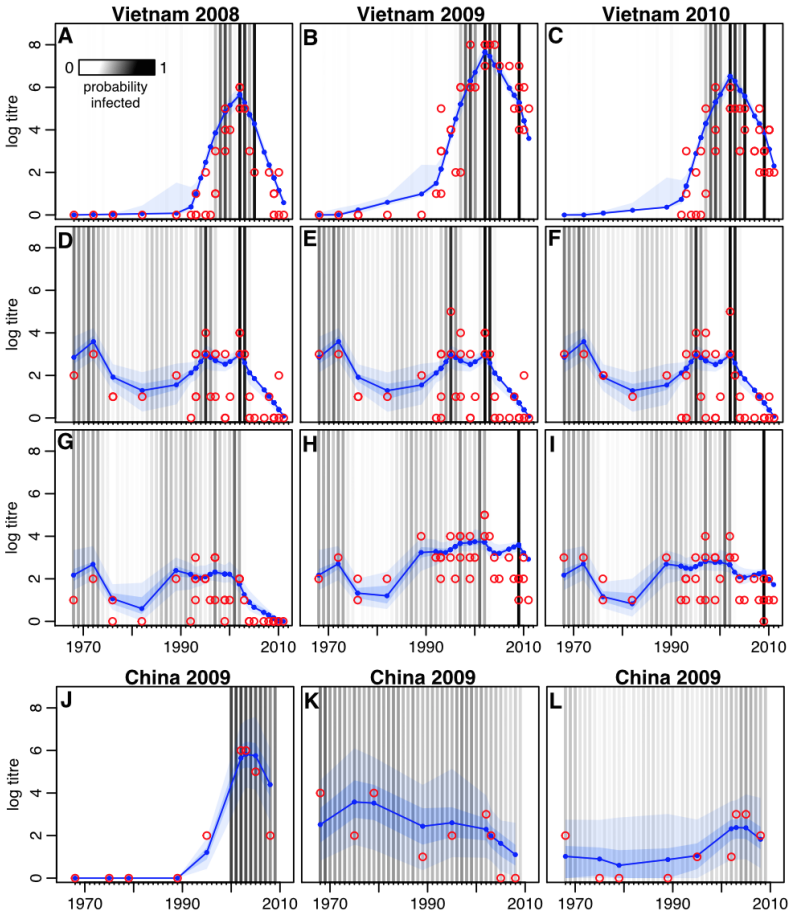

Figure 1: **Representative individual-level responses against influenza in Vietnam (A–I) and southern China (J–L). (A–C)** Strong evidence of infection in 2009, leading to rise in titres and back boost from broad short-term cross-reaction, then decay in following year. Red points show observed titre. Blue lines show median titre in fitted model, with blue regions showing 50% and 95% MCMC credibility intervals. Black lines show samples from the posterior distribution of individual infection histories, with opacity indicating the probability of infection (i.e. proportion of MCMC samples that estimated infection in that year). **(D–F)** No estimated infections between 2008–2010, so titres are at equilibrium. **(G–I)** Infection in 2009 leading to broad boost, with titres generally highest against recent strains **(H)** then decline to equilibrium, with lower mean titres against recent strains as a result of antigenic seniority **(I)**. **(J–L)** Cross-sectional results from southern China, indicating: **(J)** evidence of multiple recent infections; **(K)** decline in titres as a result of antigenic seniority; **(L)** evidence of infections early and late in life.

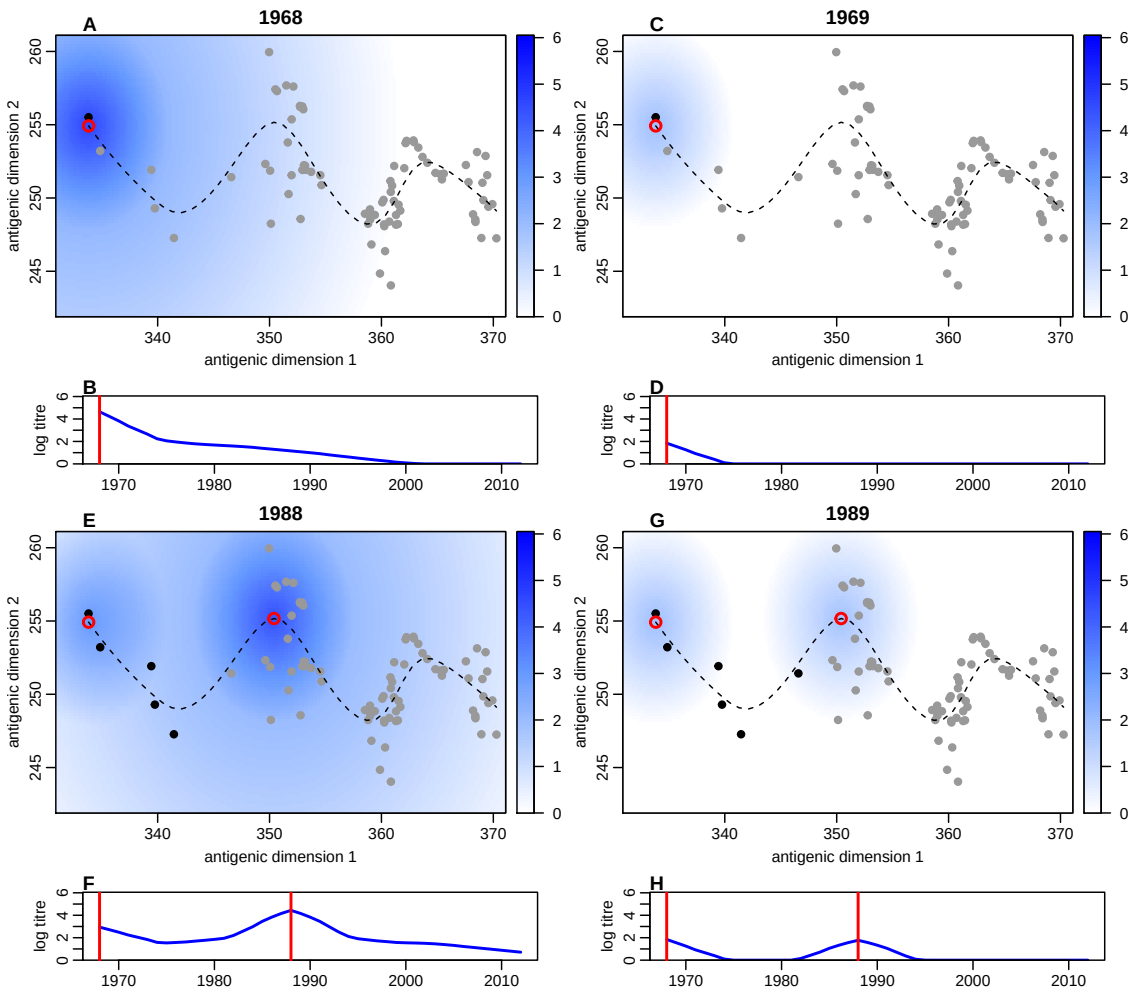

Figure 2: **Expected titres against strains at different points in antigenic space. (A)** Simulated log-titres against different strains in antigenic space following a single infection in 1968, with test conducted in 1968. Parameters are drawn from the maximum a posteriori model estimate. Black points show location of strains isolated up to this year; grey points show location of strain isolates in subsequent years, red points show location of infections. Black dashed line shows antigenic summary path used to fit model (Figure S1). **(B)** Estimated titres along the antigenic summary path. Red line shows year of infection. **(C)** Simulated log-titres following on single infection in 1968, with test conducted in 1969. **(D)** Estimated titres along antigenic summary path in 1969. **(E)** Simulated log-titres following infections in 1968 and 1998, with test conducted in 1998. **(F)** Estimated titres along antigenic summary path in 1998. **(G)** Simulated log-titres following infections in 1968 and 1998, with test conducted in 1999. **(H)** Estimated titres along antigenic summary path in 1999.

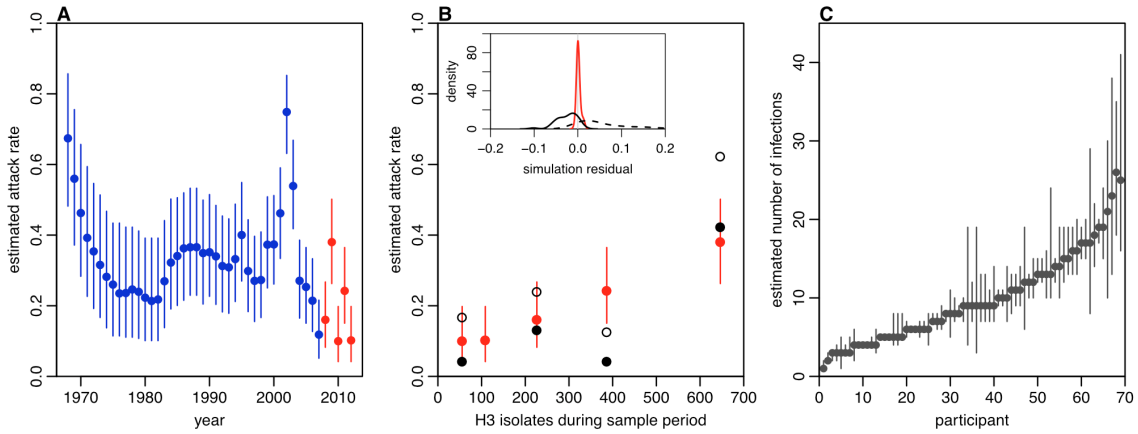

Figure 3: **Estimated attack rates for influenza A/H3N2 in Vietnam. (A)** Proportion of population estimated to have been infected in each year. Blue lines show estimated attack rate with binomial confidence interval; red lines show attack rates in years when samples were taken. **(B)** Accuracy of attack rates estimates using different methods. Main plot shows model estimates of attack rates in 2008–2012 (red points in **(A)**) and number of positive H3 isolates reported in Vietnam during the same intervals as the samples were taken. Hollow black points show attack rate based on two-fold rise in titre against strain in that year (point not shown for 2012 as no test strains for this year were available, so a rise could not be calculated); solid points show attack rate based on four-fold rise. Inset shows distribution of differences between estimated and actual attack rates in 2008–12 in simulation studies. Red line indicates estimates from joint model; dashed black line shows estimates based on two-fold rise in titre; solid black line shows estimates based on four-fold rise. **(C)** Distribution of estimated number of infections for each individual, with median and 95% credible interval show.

Supplementary Materials: Timescales of influenza A/H3N2 antibody dynamics

Materials and Methods

Serological data

We used two publicly available datasets in our analysis. In the southern China data, cross-sectional serology was taken in 2009 from 151 participants in Guangdong province in southern China and tested using microneutralization assays against a panel of nine strains: six vaccine strains (A/Hong Kong/1/1968, A/Victoria/3/1975, A/Bangkok/1/1979, A/ Beijing/353/1989, A/Wuhan/359/1995, and A/Fujian/411/2002) and three strains that circulated in southern China in recent years preceding the study (A/Shantou/90/2003, A/Shantou/806/2005, and A/Shantou/904/2008) (*13, 16*). The Vietnam data included longitudinal serology collected between 2007–2012 from 69 participants in Ha Nam (*17*), with sera tested using haemagglutination inhibition (HI) assays against a panel of up to 57 A/H3N2 strains isolated between 1968–2008 (*9*). All of the Vietnam participants were unvaccinated against influenza, and 19% of the southern China participants reported prior influenza vaccination.

In analysis of both datasets, we represented antibody responses by log-titre. For a titre dilution of $10 \leq D \leq 1280$, log-titre was defined as $\log_2\left(\frac{D}{10}\right) + 1$. The minimum detectable titre in both datasets was 10, so a dilution <10 was defined to have a log-titre of 0. The maximum observable titre in both datasets was 1280, which corresponded to a log-titre of 8. There were nine possible observable log-titres in our analysis, ranging from 0 to 8. The antigenic summary path used to represent strains in our analysis was generated by fitting a two-dimensional smoothing spline through 81 points representing the published estimated locations of strains in 'antigenic space' (*9*) (Fig. S1).The positions of strains in such a space depends on the distance between influenza antigens and reference antisera as measured by titre in an HI assay (*18*). In the model, we assumed that strains circulating between 1968 and 2012 were uniformly distributed along this summary path.

Model of expected titre given infection history

We expanded a previous modelling framework designed for cross-sectional data (*10*) to include short- and long-term dynamics. For an individual who had previously been infected with strains in the set X, the expected log-titre against strain j depended on five specific antibody processes:

1. Long-term boosting from infection with homologous strain. If an individual had been infected with only one strain, they would exhibit a fixed log-titre against that strain, controlled by a single parameter, μ_1.

2. Antigenic seniority acting via suppression of subsequent responses as a result of prior immunity. The titre against a particular strain was scaled by a factor $s(X, j) = \max\{0, 1-\tau(N_j-1)\}$, where N_j is the number of the strain in the infection history (i.e. the first strain is 1, the second is 2 etc.) and $|X|$ is the total number of infections, and τ was a parameter to be fitted.

3. Cross-reactivity from antigenically similar strains. As titres were on a log scale, we assumed the level of cross-reaction between a test strain j and infecting strain $m \in X$ decreased linearly with antigenic distance. This was controlled by $d_1(j, m) = \max\{0, 1 - \sigma_1\delta_{mt}\}$, where δ_{mt} was the two-dimensional Euclidean antigenic distance between strains j and m (Fig. S1), and σ_1 was a parameter to be fitted.

4. Short-term boosting, which waned over time. For an infecting strain m, this process was controlled by $\mu_2 w(m) = \mu_2 \max\{0, 1 - \omega t_m\}$, where μ_2 was a boosting parameter and ω was a waning parameter to be fitted, and t_m was the number of years since infection with strain m. We constrained $\omega \leq 1$ when fitting the model to ensure identifiability, as $\omega = 1$ or $\omega > 1$ implies that $w(m) = 0$ for all $t_m > 0$.

5. Cross-reactivity for the short-term response. The level of cross-reaction between a test strain j and infecting strain m was given by $d_2(j, m) = \max\{0, 1-\sigma_2\delta_{mt}\}$, where δ_{mt} was the antigenic distance between strains j and m, and σ_2 was a parameter to be fitted.

To combine the five processes in the model, we assumed that the expected log-titre individual i had against a strain j was a linear combination of the responses from each prior

infection:

$$\lambda_{ij} = \sum_{m \in X} s(X, m) \left[\mu_1 d_1(j, m) + \mu_2 w(m)\, d_2(j, m)\right] \tag{1}$$

Depending on parameter values, our model could incorporate several specific mechanistic features, including: long-term response only ($\mu_2 = 0$); waning response only ($\mu_1 = 0$); or long-term/short-term boosting independent of a cross-reactive memory response ($\sigma_1, \sigma_2 = 0$).

Observation model and likelihood function

For an individual i who was infected with strains in the set X, we assumed their true titre against strain j titre followed a normal distribution with mean λ_{ij}, standard deviation ε, and cumulative distribution function $f(x)$. The observed distribution of titres was censored to account for integer valued cutoffs. The likelihood of observing titre $k \in \{0, ..., 8\}$ given history X and parameter set θ was therefore as follows:

$$L(k \mid \theta, X) = \begin{cases} f(x < 1) & \text{if } k = 0; \\ f(k \leq x < k+1) & \text{if } 1 \leq k < 8. \\ f(x \geq 8) & \text{if } k \geq 8; \end{cases} \tag{2}$$

Parameter estimation

We fitted the model to serological data using Markov chain Monte Carlo (MCMC). Using the likelihood function in Equation 2, we jointly estimated θ across all individuals and estimated X for each individual via a Metropolis-Hastings algorithm. If individual sera were collected in more than one year, parameters were jointly estimated across all test years. We used a data augmentation approach to estimate individual infection histories. Every second iteration, we resampled model parameters, which were shared across all individuals, and performed a single Metropolis-Hastings acceptance step. On the other iterations we resampled infection histories for a randomly selected 50% of individuals. These histories were independent across individuals, so we performed a Metropolis-Hastings acceptance step for each individual separately. Correlation plots indicated that all parameters in the full model were identifiable (Fig. S9).

To ensure the Markov chain was irreducible, resampling at each step involved one of the following: addition of infection in some year; removal of infection in some year;

moving an infection from some year to another (*34*). We also used adaptive MCMC to improve the efficiency of mixing: at each iteration, we adjusted the magnitude of the covariance matrix used to resample θ to obtain an acceptance rate of 0.234 (*35*). As we had data on participants individual ages in the southern China data, we constrained potential infections in the model to years in which participants would have been alive. The model was implemented in R version 3.3.1 and C, and used the Rcpp and doMC packages. Source code and data are available at: https://github.com/adamkucharski/flu-model/

Simulation study

In our simulation study, we first generated simulated influenza attack rates between 1969–2012 using a lognormal distribution with mean 0.15 and standard deviation 0.5. For 1968, we used a lognormal distribution with mean 0.5, to reflect higher incidence in the pandemic year (*36*). Using these simulated attack rates, we generated individual infection histories for 69 participants using a binomial distribution, then generated observed individual level titres against the same strains as in the Vietnam dataset using our titre model. As in the real data, simulated samples were tested each year between 2007–2012. We assumed $\mu_1 = \mu_2 = 2$, $\tau = 0.05$, $\omega = 1$, $\sigma_1 = 0.3$, $\sigma_2 = 0.1$ and $\varepsilon = 1$ in simulations. For Fig. 3B, we simulated 10 independent sets of observed titres, then inferred the proportion of the population infected in the four years between 2008–2011 inclusive. The resulting distribution of model residuals (i.e. estimated minus actual simulated value) for these 40 data points were plotted as kernel density plots.

Epidemiological data

Reported influenza A/H3N2 activity in Vietnam was obtained from the WHO FluNet database (*37*) (Fig. S10). We aggregated reports into temporal windows based on dates of serological sample collection (*9*), and used the cumulative number of isolates in each period to compare observed activity with model estimates. To calculate attack rates from the model outputs, we scaled the posterior distribution of total number of infections across all participants for each year between 1968–2012 by the proportion of participants who were alive in that year, which we calculated based on the age distribution of participants. This produced the estimates in Figs. 3A–B.

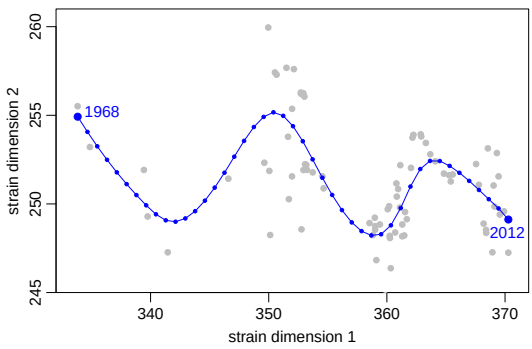

Figure S1: **Assumed antigenic locations of historical strains in model between 1968 and 2012 (blue dots).** These locations were generated by using a spline to estimate a 'summary path' of influenza antigenic drift (blue line) from the antigenic locations of strains isolated during this period (shown as grey dots) (*9*).

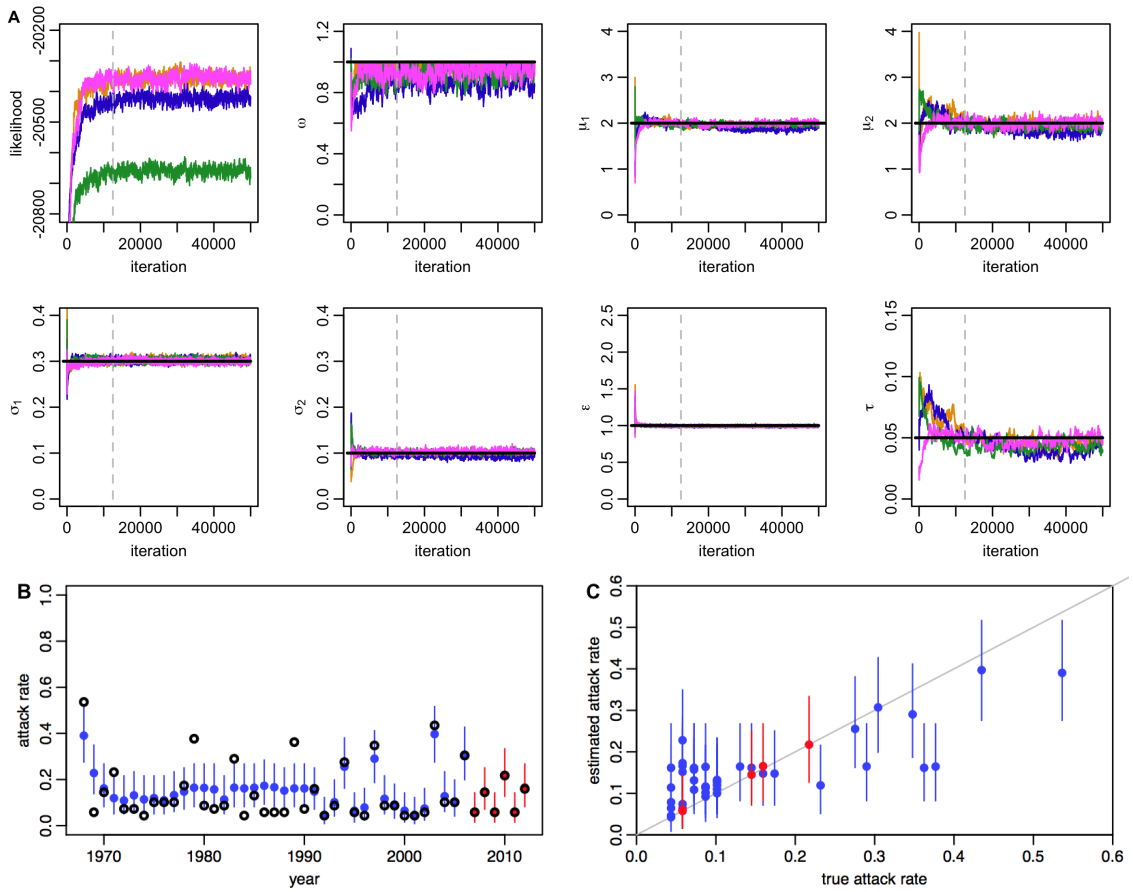

Figure S2: **Simulation study posterior results.** Inference performed using simulated data for 69 participants, with same strains as tested in HaNam data (57 in total, including repeats in some years). **(A)** Convergence plots for 4 MCMC runs are shown. Note that each run used a different simulation dataset, so the likelihoods are not directly comparable. **(B)** Comparison of simulated and true attack rates for one of the chains. Blue lines show estimated attack rate with binomial confidence interval; red lines show attack rates in years when samples were taken. Similar results were obtained for all four chains. **(C)** The accuracy of attack rate estimates was better for recent years (shown as red dots) which were more densely sampled in the serological data.

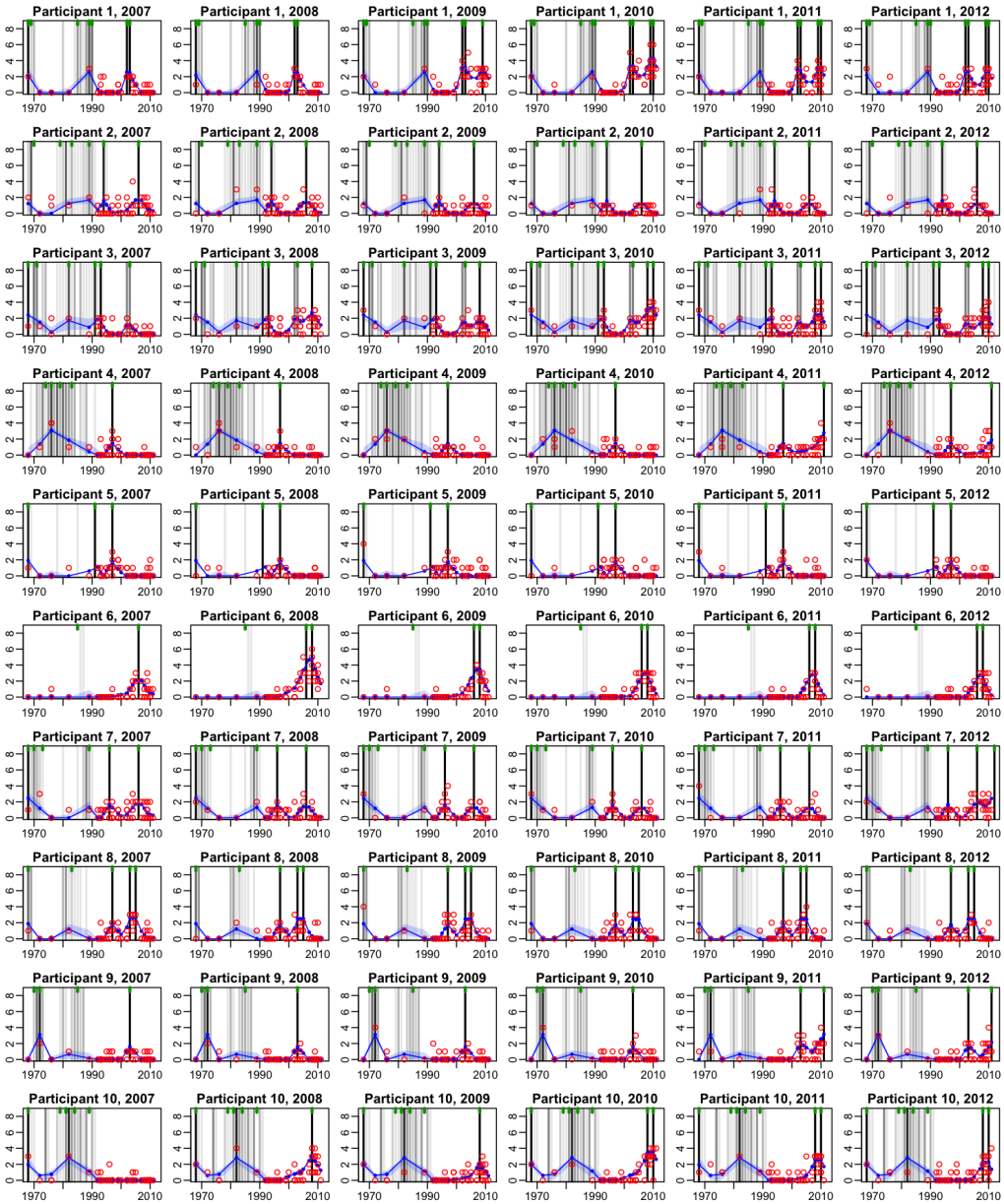

Figure S3: **Selection of 10 individual estimated histories for simulated data.** Red points show observed titre. Blue lines show median titre in fitted model, with blue regions showing 50% and 95% MCMC credibility intervals. Black lines show samples from the posterior distribution of individual infection histories, with opacity indicating the probability of infection (i.e. proportion of MCMC samples that estimated infection in that year). Green lines show true years of infection in simulation.

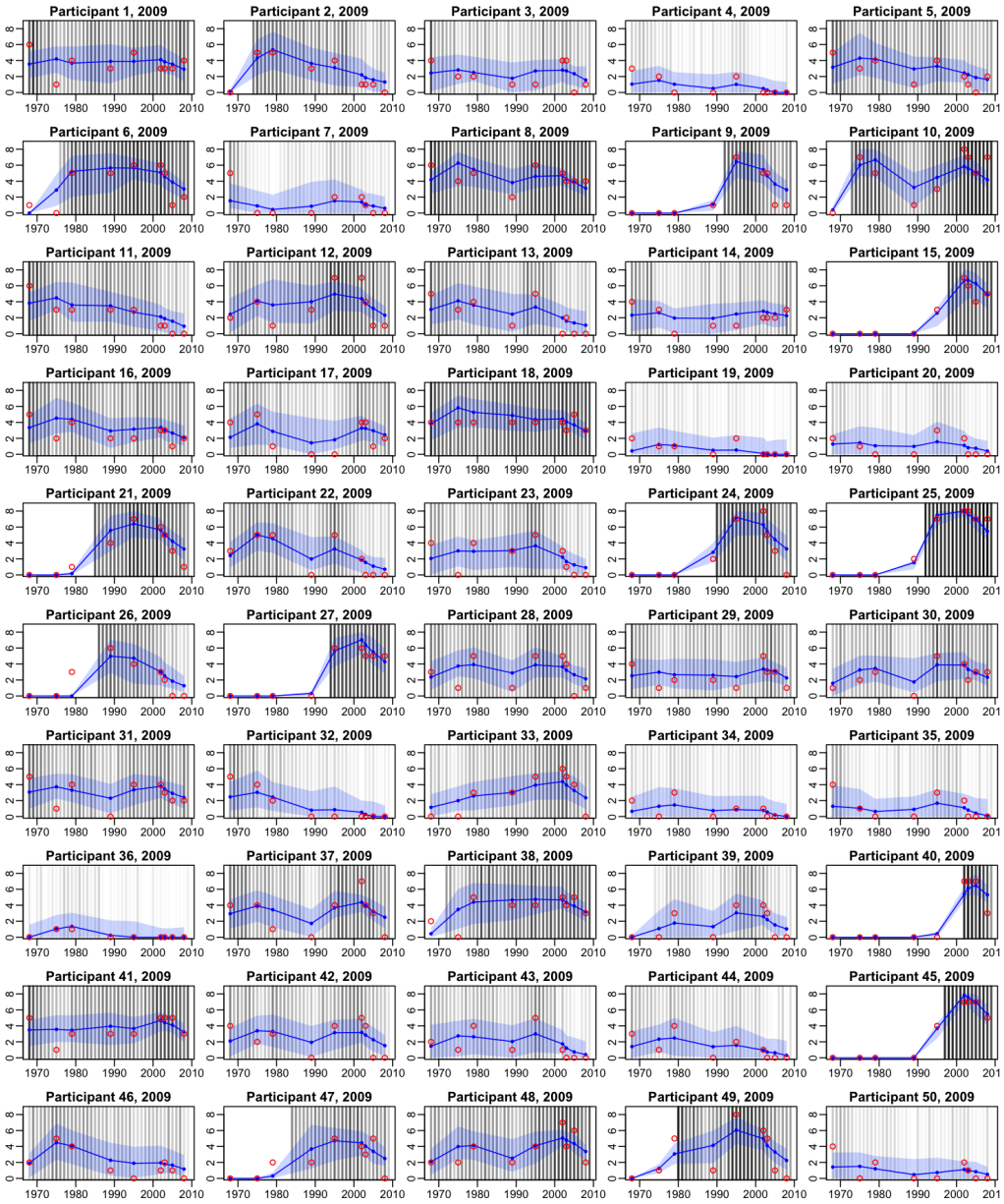

Figure S4: **Selection of 50 individual estimated histories for A/H3N2 FluScape data.**

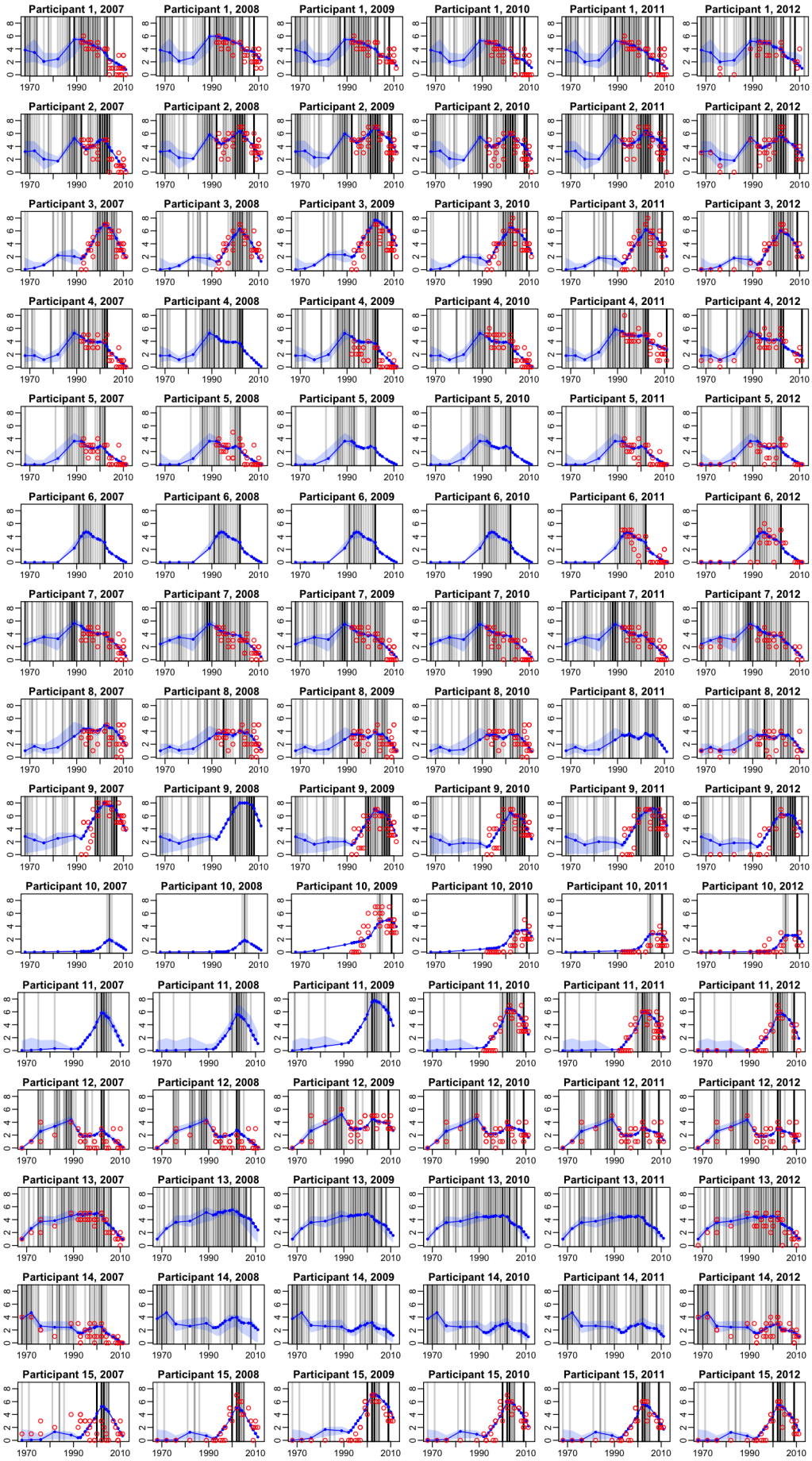
Participant 1, 2007
Participant 1, 2008
Participant 1, 2009
Participant 1, 2010
Participant 1, 2011
Participant 1, 2012
Participant 2, 2007
Participant 2, 2008
Participant 2, 2009
Participant 2, 2010
Participant 2, 2011
Participant 2, 2012
Participant 3, 2007
Participant 3, 2008
Participant 3, 2009
Participant 3, 2010
Participant 3, 2011
Participant 3, 2012
Participant 4, 2007
Participant 4, 2008
Participant 4, 2009
Participant 4, 2010
Participant 4, 2011
Participant 4, 2012
Participant 5, 2007
Participant 5, 2008
Participant 5, 2009
Participant 5, 2010
Participant 5, 2011
Participant 5, 2012
Participant 6, 2007
Participant 6, 2008
Participant 6, 2009
Participant 6, 2010
Participant 6, 2011
Participant 6, 2012
Participant 7, 2007
Participant 7, 2008
Participant 7, 2009
Participant 7, 2010
Participant 7, 2011
Participant 7, 2012
Participant 8, 2007
Participant 8, 2008
Participant 8, 2009
Participant 8, 2010
Participant 8, 2011
Participant 8, 2012
Participant 9, 2007
Participant 9, 2008
Participant 9, 2009
Participant 9, 2010
Participant 9, 2011
Participant 9, 2012
Participant 10, 2007
Participant 10, 2008
Participant 10, 2009
Participant 10, 2010
Participant 10, 2011
Participant 10, 2012
Participant 11, 2007
Participant 11, 2008
Participant 11, 2009
Participant 11, 2010
Participant 11, 2011
Participant 11, 2012
Participant 12, 2007
Participant 12, 2008
Participant 12, 2009
Participant 12, 2010
Participant 12, 2011
Participant 12, 2012
Participant 13, 2007
Participant 13, 2008
Participant 13, 2009
Participant 13, 2010
Participant 13, 2011
Participant 13, 2012
Participant 14, 2007
Participant 14, 2008
Participant 14, 2009
Participant 14, 2010
Participant 14, 2011
Participant 14, 2012
Participant 15, 2007
Participant 15, 2008
Participant 15, 2009
Participant 15, 2010
Participant 15, 2011
Participant 15, 2012
0 2 4 6 8
1970 1990 2010

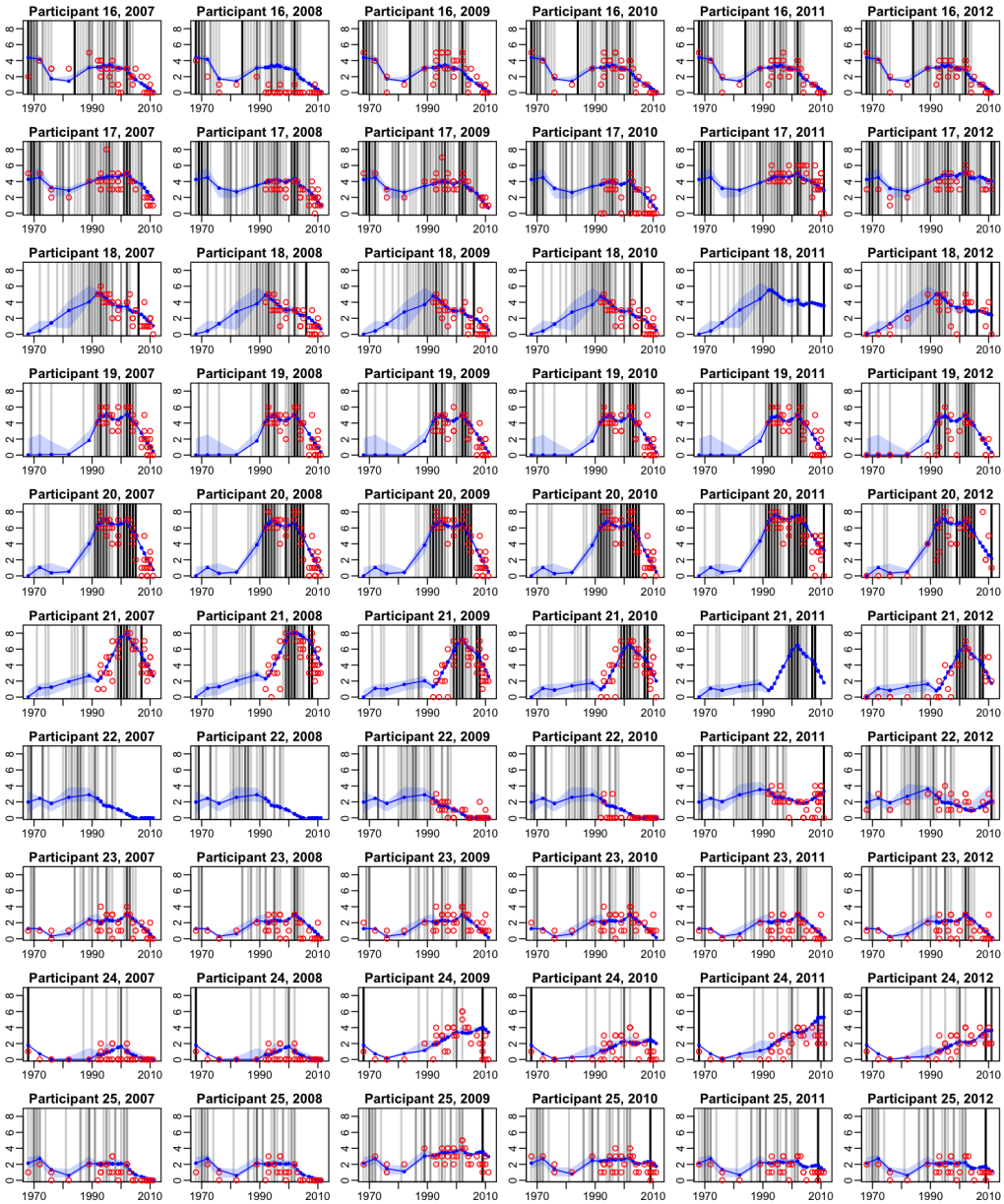

Figure S5: **Selection of 25 individual estimated histories for A/H3N2 Vietnam data.**

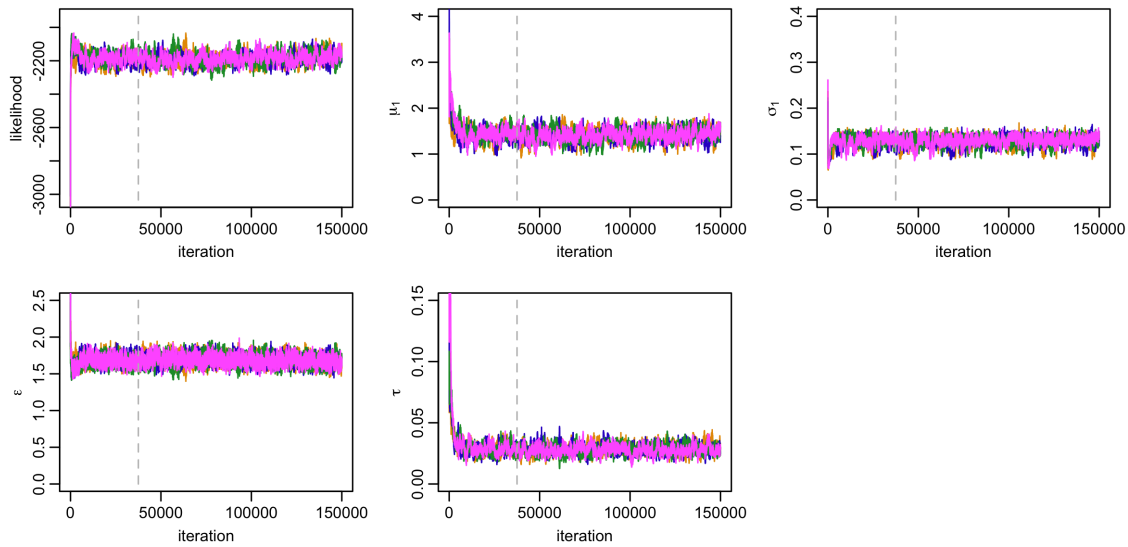

Figure S6: **MCMC diagnostics for 4 chains fitted to A/H3N2 FluScape data.** Dashed line shows burn in period.

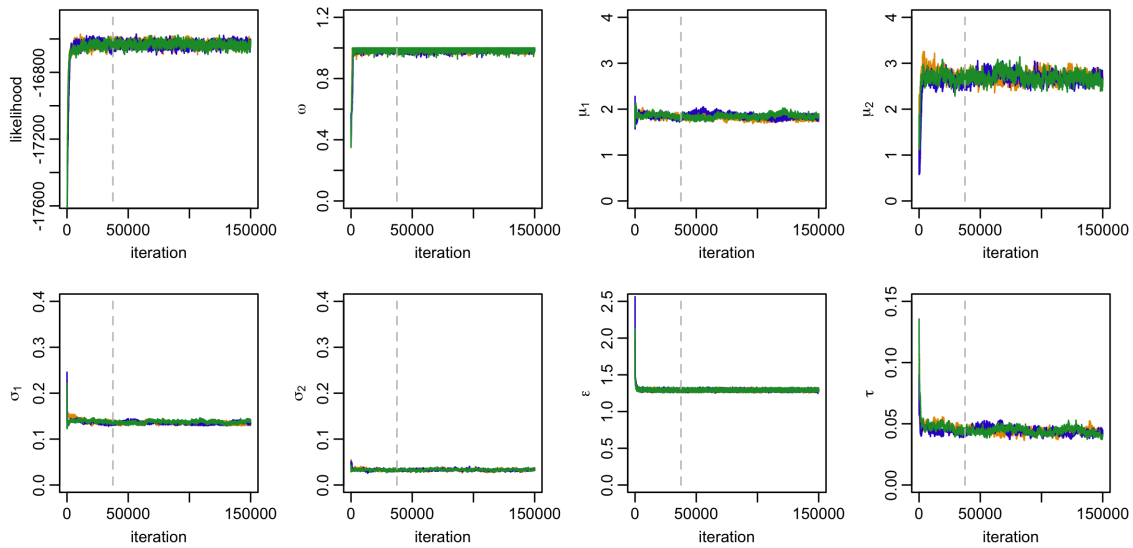

Figure S7: **MCMC diagnostics for 3 chains fitted to A/H3N2 Vietnam data.** Dashed line shows burn in period.

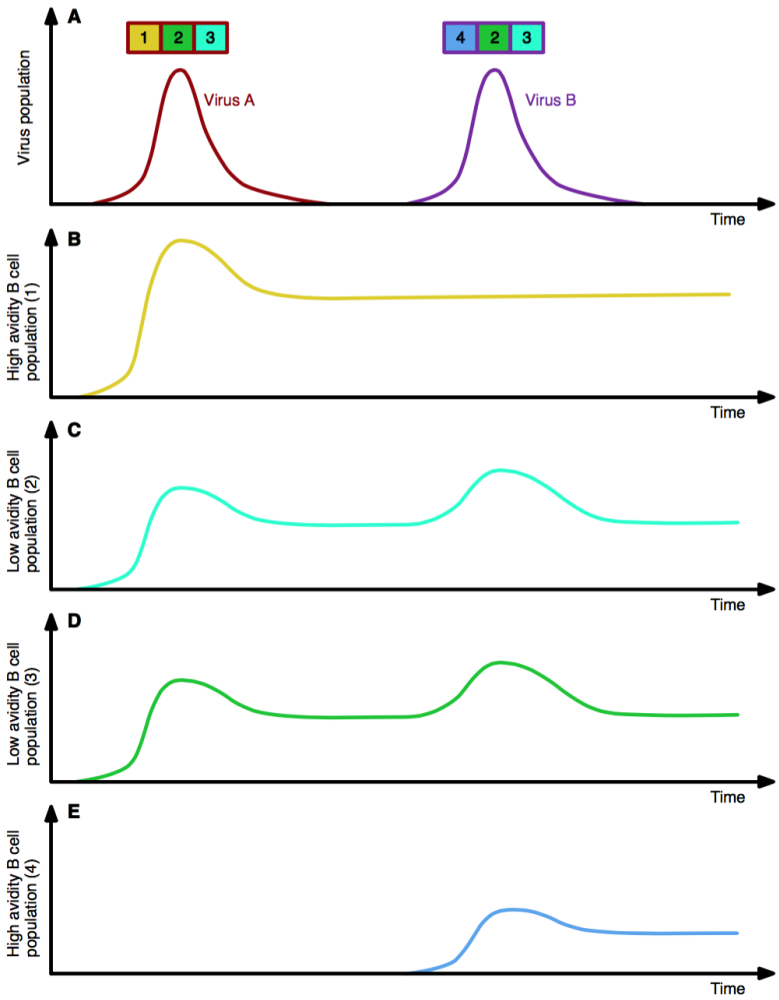

Figure S8: **Schematic of two-armed immune response against sequential influenza viruses.** **(A)** In this simple illustration, each virus has three epitopes that can be targeted by monoclonal antibodies. The first infection, with virus A, stimulates distinct populations of memory B cells within the host that produce **(B)** antibodies with high avidity to epitope 1, and **(C–D)** antibodies with lower avidity to epitopes 2 and 3. After clearance of virus, these B cell populations decline to an equilibrium level. Upon secondary infection with virus B – which has epitopes 2 and 3 but with a new epitope 4 in place of epitope 1 – the lower avidity B cell populations are activated, along with **(E)** a newly stimulated B cell population that has high avidity to epitope 4. However, the virus population is neutralised before these B cells reach the level of earlier B cell populations, which produce the 'antigenic seniority' effect. Following the secondary infection, the host would exhibit raised levels of antibodies against epitopes 2 and 3, and hence produce a response even against viruses with only one of these epitopes. This results in a short-lived broadly cross-reactive response, which wanes to leave a narrower long-term response.

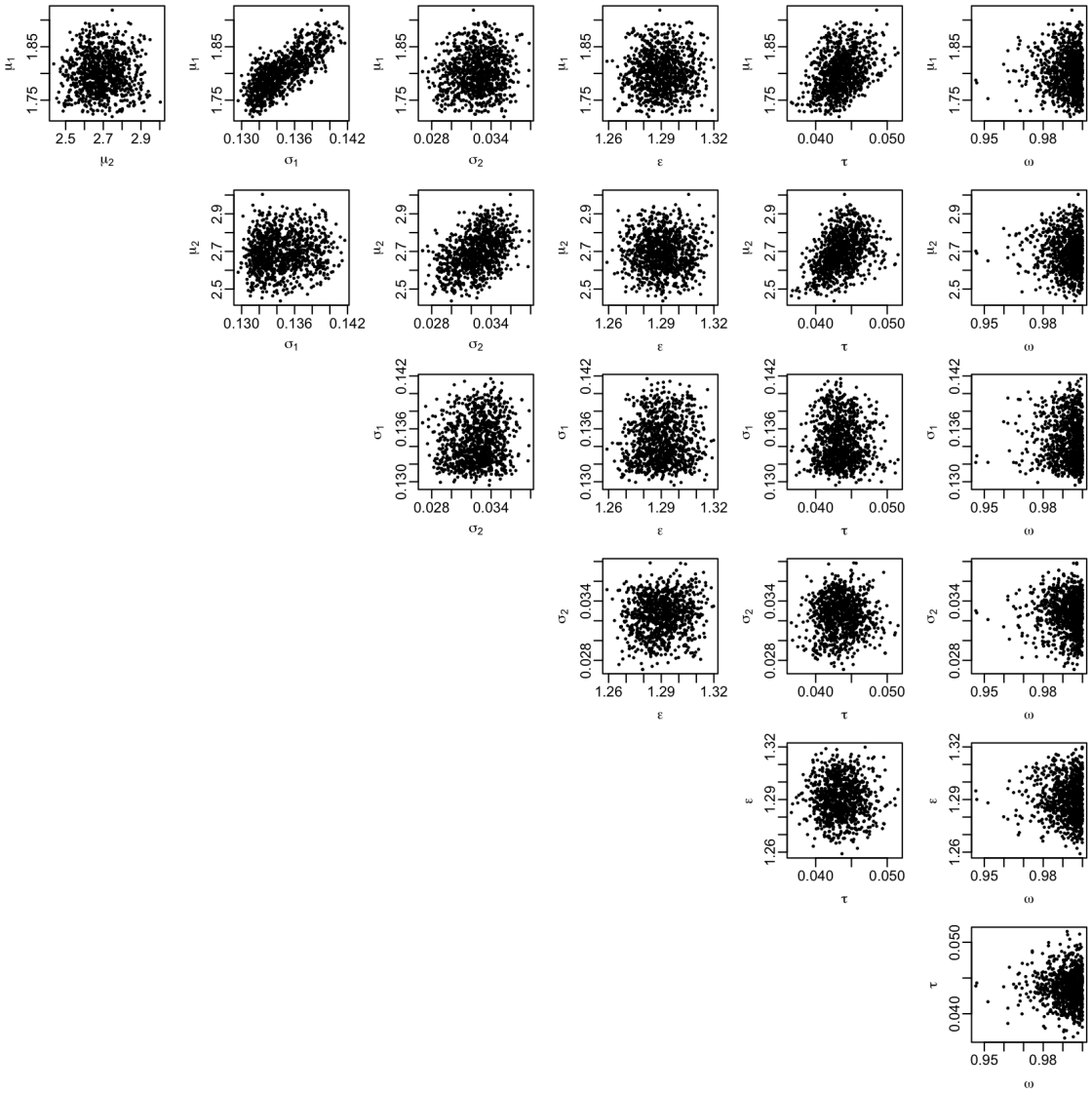

Figure S9: **Correlation plots for parameter estimates using A/H3N2 Vietnam data.** Pairwise plots show 1000 MCMC samples from the full joint posterior distribution.

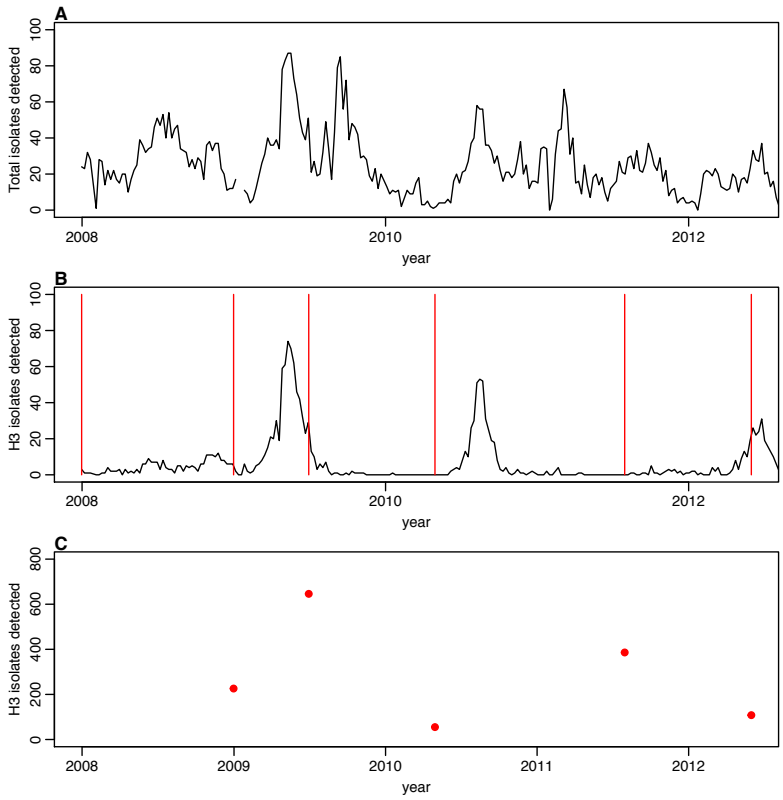

Figure S10: **Vietnam weekly influenza isolates.** **(A)** All influenza isolates reported (*37*). **(B)** A/H3N2 isolates. Red lines show times of serological sampling. **(C)** Cumulative isolates in each period.

Dataset	Residuals ≤ 1	Residuals ≤ 2	Residuals ≤ 3
China 2009	0.78	0.95	0.99
Vietnam 2007-2012	0.57	0.77	0.90

Table S1: **Proportion of estimated titres with model residuals less than 1, 2 and 3, based on the distribution in Fig. S6.**

Parameter	China (2009)	ESS	Vietnam (2007–2012)	ESS
Long-term boost (μ_1)	1.42 (1.12-1.67)	132	1.8 (1.74-1.88)	248
Short-term boost (μ_2)	–	–	2.69 (2.5-2.89)	191
Long-term cross-reaction (σ_1)	0.128 (0.102-0.145)	203	0.134 (0.131-0.14)	193
Short-term cross-reaction (σ_2)	–	–	0.0327 (0.0287-0.036)	125
Observation error (ε)	1.69 (1.55-1.83)	360	1.29 (1.27-1.31)	4860
Antigenic seniority (τ)	0.029 (0.021-0.037)	232	0.0435 (0.0389-0.0481)	100
Waning (ω)	–	–	0.995 (0.973-1)	3810

Table S2: **Parameter estimates for models fitted to data from southern China and Vietnam.** Median estimate shown, with 95% credible interval in parentheses. Effective sample size (ESS) for each parameter is also shown, to indicate the extent of autocorrelation in MCMC sampling. The estimated error structure of the two assays suggests that for a log-titre mid-way between two integer cutoffs (e.g. 1.5), there was a 0.233 (0.216–0.253) probability that the microneutralisation test would return the correct log-titre measurement (i.e. 1), and 0.302 (0.297–0.306) probability of a correct observation in the HI assay.